Microstructure characterization of rapidly solidified Al-Mg-Sc with Li droplets

T. Gancarz[1,#], A-A. Bogno[2], K. Berent[3], G. Cempura[4], N. Schell[5], R. Chulist[1], H. Henein[2]

[1]*Institute of Metallurgy and Materials Science, Polish Academy of Sciences, Reymonta 25 St., 30-059 Krakow, Poland*

[2] *AMPL, Department of Chemical and Materials Engineering, University of Alberta, Canada*

[3] *AGH University of Science and Technology, Academic Centre for Materials and Nanotechnology, Mickiewicza 30 Av., 30-059 Krakow, Poland*

[4] *AGH University of Science and Technology, International Centre of Electron Microscopy for Materials Science, Faculty of Metals Engineering and Industrial Computer Science, Krakow, Poland*

[5] *Institute of Materials Research, Helmholtz-Zentrum Geesthacht, Max-Planck-Strasse 1, D-21502 Geesthacht, Germany*

- Corresponding author t.gancarz@imim.pl, tel. +48 122952824, fax. +48 122952804

Abstract

In the case of increasing possibility of application Al alloys the Al5.0Mg0.2Sc alloy with 3.0 and 6.0 Li (wt %) after atomisation process was proposed in this study. To characterise liquid alloys the discharge crucible method was used, which allow to determine density, surface tension and viscosity with temperature dependency. The experimental results show that the density and surface tension are decreasing with Li content, opposite to viscosity which increasing, what probably is caused by short-range ordering from occurring intermetallic phases. The obtained powder after atomisation process was subjected using calorimeter for design characteristic temperatures, and the microstructure observation and chemical analysis was conducted using scanning and transmission electron microscopy with energy dispersive X-ray spectroscopy. To identify the occurring phases in the study alloys was performed the diffraction pattern in transmission electron microscopy and X-ray diffraction using synchrotron measurements. The conducted measurements and microstructure observation

show occurring Al_3Sc and Al_2MgLi phases in both alloys and AlLi in Al5.0Mg0.2Sc6.0Li alloy, which is in the line with a phase diagram.

Keywords: Al alloys; Rapid solidification; Impulse atomization; Synchrotron; Electron backscattered diffraction; Microstructure

Introduction

The Al alloys (series 2xxx, 5xxx or 7xxx) are attracting renewed interest due to the search for weight reductions and better mechanical properties for the aerospace and automotive industry [1, 2]. The applied the precipitation hardening by addition Li, Sc, Zr or Ti is one of the most potent ways to increase the strength of aluminium alloys and is used extensively in transportation applications. The obtaining stable nanostructure of precipitates requires steps of phase nucleation and diffusion-controlled growth [3]. For the mechanical properties is responds the coherency between these hardening precipitates and the matrix and the reducing of this correlation can be caused by a pronounced decrease of the strength of these alloys, which can be promoted by deformation, heating or aging especially results in an effective grain refinement during casting, cold or hot working [2, 4]. Taking into account the are needed new methods of production, for rapid solidification which takes place at the interface between the atmosphere and liquid subsequently solid and liquids phases. When the interface follows non thermodynamic equilibrium, its growth is mainly controlled by rapid crystallization [5]. Using the rapid solidified techniques resulting in higher toughness, higher hardness, better wear resistance, better fatigue resistance or improved corrosion resistance [6, 7]. The higher properties are correlated with the morphology of microstructure which is caused non-equilibrium phase formation [7]. Rapid solidification technic allows to from liquid metal extrusion or formation of powder, wire, filament or ribbon type product [8]. For

the production of powder the impulse atomization (IA) technique was developed [9] and the process of production powder from Al alloys was characterized in a previous study [7, 10-13].

According to Al alloys, scandium contributes significantly to improving strength by forming nanoscale coherent Al_3Sc precipitates [2, 14, 15]. However, the additions of ternary elements as Mg to Al-Sc system, improving the mechanical properties and nanostructural stability [2, 14]. In the [14] are presented the effects of Mg additions on Al_3Sc precipitation in Al–Sc alloys, which is important for optimizing the mechanical properties of these multicomponent alloys, and also the influence of Mg for creep behavior of Al(Sc) based. The results show that the Mg segregation occurring at the perfectly coherent α-Al/Al3Sc heterophase interface, which is kinetically trapped since Mg is insoluble in Al_3Sc [14]. Therefore the segregation of Mg leads to a substantial reduction in the anisotropy of the α-Al/Al_3Sc interfacial free energies, what was confirmed by HREM observations [14]. This behaviour is correlated with oversized Mg atom 12.08% by radius and 40.82 by volume [16] in solid solution in the a-Al matrix. On the other hand in the Al-Mg-Li system [1] during fast quench to room temperature and low temperature ageing the Al_3Li phase precipitations was dominated, which are coherent with the Al matrix. The second phase of this system is ternary phase S1-Al_2MgLi which mostly nucleated heterogeneously on grain boundaries or dispersoids. The main reason for the enhancement of precipitation in the Al–Li system with an addition of Mg is a decrease in the solubility of Li in the Al matrix, whereas the interfacial energy of the precipitates is not significantly changed, nor the diffusivity of Li in Al [1]. According to the quaternary system Al-Mg-Li-Sc the Sc addition increases the stability of the solid solution and the hardenability of alloys containing lithium due to the changed Mg/Li proportion in the solid solution [17]. However, the increase in the cooling rate in quenching increases the capacity for corrosion cracking of Al-Li alloys, which requires restriction of not only the lower limit of the cooling rate but also its upper limit [17].

The aim of the present work is to present results of the advanced characterization of a large number of Al–Mg-Sc-Li droplets formed by the IA technique using scanning and transmission electron microscopy, and diffraction of high-energy synchrotron radiation. To the study was selected Al-5.0Mg-0.2Sc with the addition of 3.0 or 6.0 Li (wt %). The influence of Mg content from 2 to 6 (wt %) in Al-Mg-Sc alloys was studied in [18] where the mechanical properties increased with increased Mg content, however, the slight differences between 4 and 6 (wt %) are observed. The level of Sc was chosen according to investigate [19] where 0.01 (wt %) Sc caused increasing mechanical properties, yield strength, a tensile strength and elongation, and also stabilized and shift to the lower temperature equilibrium of Al-Li phases. The presence of Sc leads to a significantly reduced size of the Al_3Li precipitates, but has also a limited effect on the precipitation kinetics which is resulting in increasing strength in the binary Al-Li system [20-22]. Therefore, the Sc addition has influence for precipitate depending on composition and thermomechanical processing of Li with Al and Mg phases. Such a higher of application of Al-Sc alloys are promising for automotive and air transportation applications correlate with capability of weight reduction on critical moving parts, strong bonding while welding aluminum, good corrosion resistance, however, taking into account the price of Sc caused certain strict use of this additive to achieve specific goals [23].

2. Droplet production and characterization techniques

2.1 Material

The Al-Mg-Sc-Li alloys were prepared by melting accurately weighed amounts of high-purity metals (Al, Mg and Sc 99.999%, and Li 99.95%) in a glove-box under a protective atmosphere of high purity argon, with water vapour, nitrogen and oxygen concentration lower than 0.1 ppm to avoid the oxidation of liquid alloys. To improve the atmosphere in glovebox there is a connection with high temperature cleaner with Ti shaving working at temperature

850℃, with circulation 35 m^3/h. Alloys are prepared in an electrical furnace in the Al_2O_3 crucibles, first was melt the Al with Sc at 1000℃ after melting the temperature was reduced to 800℃, then Mg and Li (with small parts) was added. Next the alloy was mixing and casted to steel plate. That prepared alloys was taken to physical properties measurements and atomization process.

2.2 *Discharge crucible method (DC)*

To design the physicochemical properties of liquid Al-Mg-Sc-Li alloys the DC method (described and shown in detail elsewhere [24]) was used. The method based on the measured weight over a given period time, the density, surface tension and viscosity can be calculated. Using the numerical solutions based on the relationship between the volumetric flow rate of liquid Q exiting the crucible through the orifice of fixed radius r_0, the head of the liquid is calculated using equation (1). Based on dependences of changing mass over time, and using the numerical solutions obtained from equation (1), density, surface tension and viscosity were calculated for each alloy.

$$h = \frac{1}{2g}\left(\frac{Q}{\left(a_4\left(\frac{2\rho Q}{\pi r_0 \eta}\right)^3 + a_3\left(\frac{2\rho Q}{\pi r_0 \eta}\right)^2 + a_2\left(\frac{2\rho Q}{\pi r_0 \eta}\right) + a_1\right)\pi r_0^2}\right) + \frac{\sigma}{\rho g r_0} \qquad (1)$$

where: ρ is the density of liquid (kg/m^3), g is gravitational acceleration (m/s^2), r_0 is the orifice radius in the bottom of crucible (m), σ is surface tension (mN/m), Q is free flow (m^3/s), η and σ are viscosity and surface tension, respectively, C_d is the discharge coefficient determined for a given crucible, based on the free flow of liquids with known density, *Re* is the Reynolds number and a1, a2, a3 and a4 are the coefficients of the polynomial describing Cd versus Re.

The obtained temperature dependence of density and surface tension were described by linear equations, and the viscosity by an Arrhenius type equation. The data are listed in

Table 1, along with estimated standard deviation of the equation parameters, and values calculated at 973 K, respectively. The line for density and surface tension and the Arrhenius equation for viscosity were in good agreement with the experimental data, and the parameter $R^2 = 0.988 \div 0.999$.

2.3. Calorimetry study

The characteristic reactions of the Al-Sc-Mg-Li alloys were investigated with differential scanning calorimetric (DSC) method using DSC 404 Netzsch. The measurements were carried out on samples of about 10 mg, with the use of DSC microcalorimeter, with heating and cooling rate of 5, 10, 20 and 40 $^{\circ}$C /min, using Al_2O_3 crucibles under a protective atmosphere of high-purity Ar (99.9999%) with flow 40 ml/min.

2.4. Droplet production

The Al5.0Mg0.2Sc alloy with 3.0 and 6.0 Li (wt %) what correspond 10.7 and 19.8 (at. %) was taken for this study. The former powder atomization studies of Al alloys have been carried out [31, 32]. The investigated droplets were produced by the impulse atomization (IA) technique, developed at AMPL (Advanced Materials & Processing Laboratory, Edmonton, Canada) [33]. The prepared alloys in special glove box (IMMS PAS in Krakow) alloys was melt in Al_2O_3 crucibles using the coil as a source of heating, after stabilizing temperature at 900 or 1000 $^{\circ}$C, the atomization process was started by mechanical impulses through a nozzle plate containing orifices of a defined diameter. The process was conducted using the gas atmosphere of either argon or helium were droplets are solidify formed form liquid by jets break down into small droplets due to the Plateau–Rayleigh instability. The obtained droplets are fully solidified before reaching an oil quench bath placed 4 m under the atomizing nozzle. This technique leads to a size distribution of the droplets, whose diameter may vary from less

than 212 μm to more than 1.4 mm in the same batch. The solidified droplets are sieved into different size classes based on the technique described in [34]. More precisely, the droplets are separated into 12 size classes, from a class containing the droplets smaller than 212 lm in diameter to a class containing the droplets larger than 1400 (μm) in diameter. The diameter range (in microns) of the 12 classes is as follows: (0–212), (212–250), (250–300), (300–355), (355–425), (425–500), (500–600), (600–710), (710–850), (850–1000), (1000-1400) and >1400.

2.3. Synchrotron X-ray identification

Phase identification was carried out using X-ray diffraction (XRD). In order to obtain information from the bulk samples, diffraction of high-energy synchrotron radiation (87.1 keV, λ = 0.142342 nm) has been performed using P07 beamline of the PETRA III at DESY (Hamburg, Germany). Transmission geometry and the high penetration depth of synchrotron radiation allow diffraction data to be obtained from representative large sample volumes. The diffraction data were collected using an area detector, located at a distance of 1070 mm from the sample, with a beam size of 0.5×0.5 mm^2. To ensure that the optimal volume of Al-Mg-Sc-Li alloy is in the beam, the sample was measured at three different sites across the interface. The most representative area was chosen for phase analysis. Additionally, to bring all grains into diffraction (all planes fulfil the Bragg condition), the sample was continuously rotated around the ω axis by -90°< ω < 90° [35]. In such a way, all orientations of a 0.5×0.5×2 mm sample volume were recorded in one single image.

2.4. Microstructure characterisation

Scanning electron microscopy (SEM), transmission electron microscopy (TEM) and electron backscattered diffraction (EBSD)

Microstructural characterization of the specimens was performed using scanning (SEM) and transmission electron microscopy (TEM) techniques. Chemical microanalysis was carried out using the energy dispersive X-ray spectroscopy (EDS) technique. EBSD measurements were conducted on a FEI Versa 3D FEG-SEM operating at 15 kV, using an EDAX-TSL OIM data Collection 7 software. Additional characterization of phase distribution was investigated by high angle annular dark field (HAADF-STEM). Phase identification was performed using selected area electron diffraction techniques (SAED), using TEM and confirmed with X-ray diffraction (XRD).

3. Results and Discussion

3.1 Liquid properties

Using DC method the physical properties of Al-Mg-Sc-Li alloys was conducted and the results are presented in Fig. 1 and collected in Table 1. The density and surface tension of Al-Mg-Sc-Li alloys is reducing with increasing Li content opposite to viscosity which is increasing. The obtained results are similar to Al-Li system where is observed the same character of changes [30]. The lowering density and increasing viscosity are correlated with short-range ordering in the liquid occurring from formed IMCs, which are described in chapter 3.3. The obtained results for pure Al shows very good agreement with literature data according to the last review by Assael et al. [36] where the difference between the proposed equation and experimental results was below 1 %. The data for similar composition Al4.6Mg0.66Sc0.42Zr0.49Mn [37] in the Fig. 1 b and c, was shown. The density and viscosity data presented in [37] were obtained by computational simulation using numerical model.

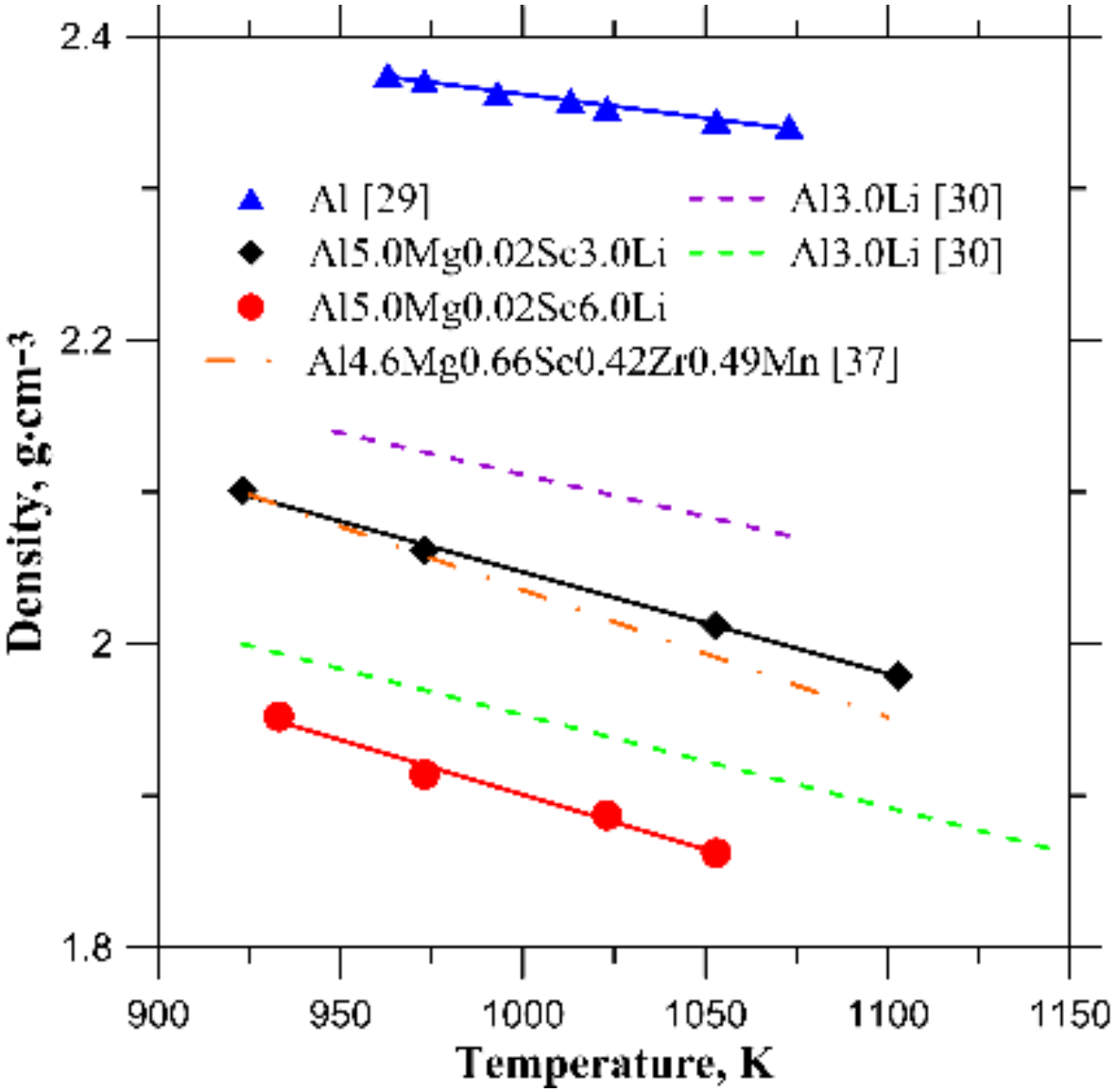
2.4
2.2
2
1.8
Density, g·cm⁻³
900
950
1000
1050
1100
1150
Temperature, K
Al [29]
Al5.0Mg0.02Sc3.0Li
Al5.0Mg0.02Sc6.0Li
Al4.6Mg0.66Sc0.42Zr0.49Mn [37]
Al3.0Li [30]
Al3.0Li [30]

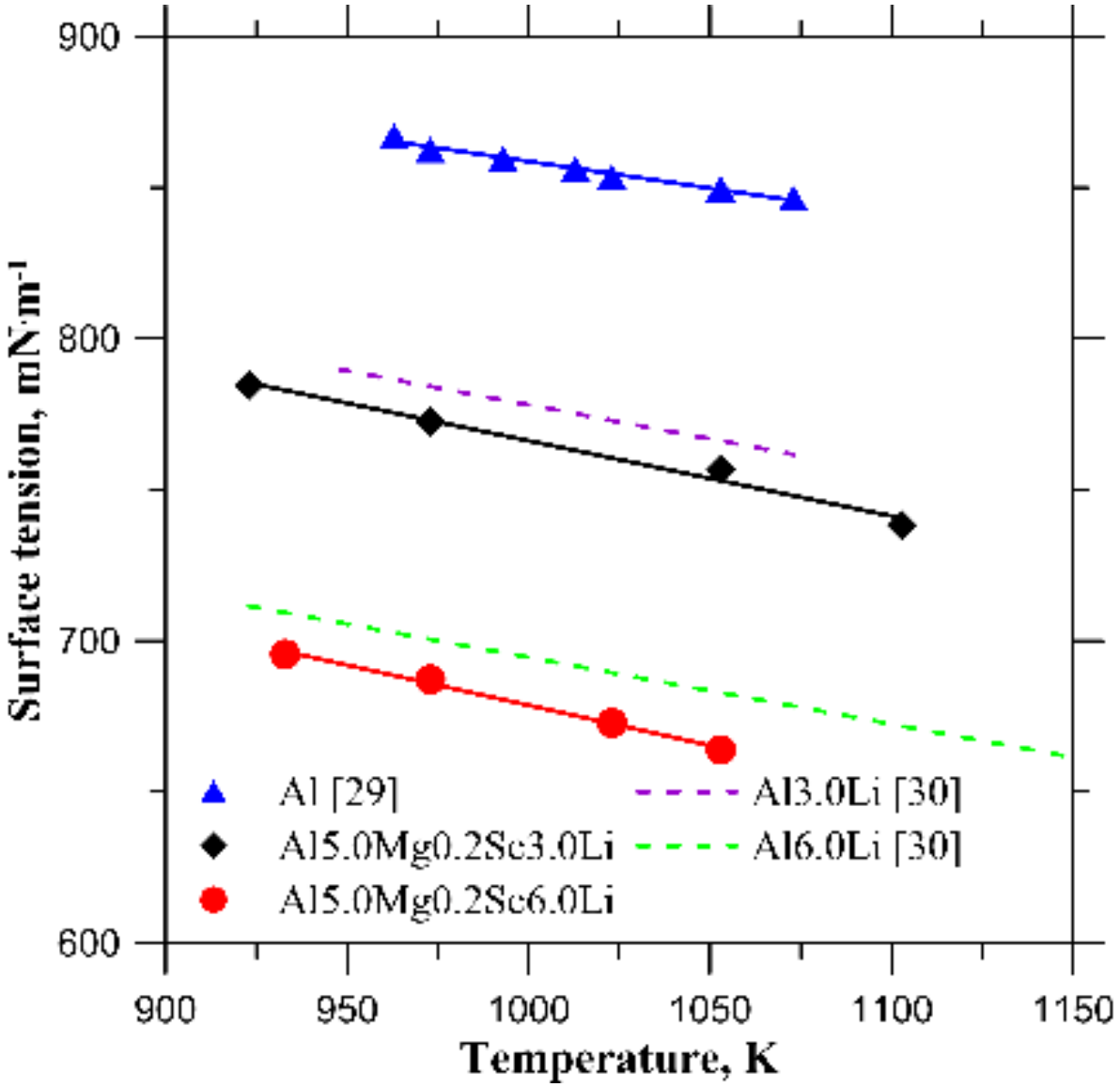
900
800
700
600
900
950
1000
1050
1100
1150
Surface tension, mN·m-1
Temperature, K
Al [29]
Al5.0Mg0.2Sc3.0Li
Al5.0Mg0.2Sc6.0Li
Al3.0Li [30]
Al6.0Li [30]

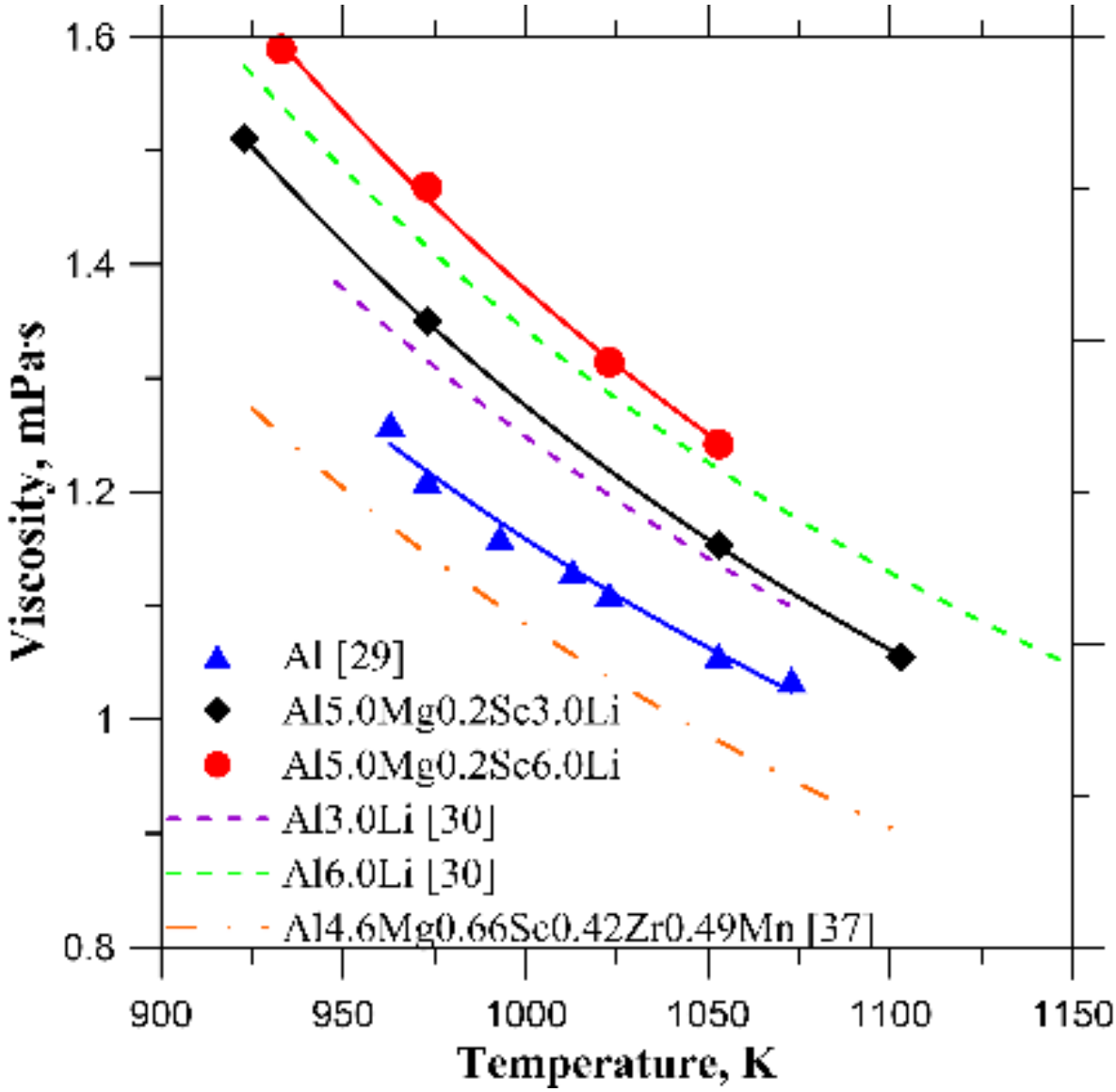

Fig. 1. The density, surface tension and viscosity of Al-Mg-Sc-Li alloys compared with literature data for Al [29], Al-Li alloys [30], and Al4.6Mg0.66Sc0.42Zr0.49Mn [37].

The density and surface tension data were described by the linear equation ($Y(T) = a + b \cdot T$), and for viscosity the Arrhenius equation ($\eta = A \cdot e^{\frac{E}{RT}}$) was used. Where Y is γ – surface tension or ρ – density, and *a*, *b* is linear parameters; η – viscosity, A, E – coefficients, R – Boltzmann constant, T – temperature.

Table 1. The A, B, E_a coefficients[a] and their standard deviation of the linear temperature dependence of density and surface tension, and the Arrhenius equation described viscosity for Al-Mg-Sc-Li alloys, and calculated values at 700 °C.

Density/ Alloys	A ($g \cdot cm^{-3}$)	u (A)	B ($g \cdot cm^{-3} T^{-1}$)	u (B)	ρ (700°C) ($g \cdot cm^{-3}$)	s (ρ)
Al [29]	2.674		-0.0003		2.371	
Al5.0Mg0.2Sc3.0Li	2.72	0.02	-0.00067	0.00002	2.233	0.003
Al5.0Mg0.2Sc6.0Li	2.62	0.06	-0.00072	0.00006	2.100	0.006
Surface tension/ Alloys	A ($mN \cdot m^{-1}$)	u (A)	B ($mN \cdot m^{-1} \cdot T^{-1}$)	u (B)	σ (700°C) ($mN \cdot m^{-1}$)	s (σ)
Al [29]	1036.10		-0.18		863.40	
Al5.0Mg0.2Sc3.0Li	1015.3	22.4	-0.249	0.022	772.9	0.2
Al5.0Mg0.2Sc6.0Li	944.7	13.9	-0.266	0.014	685.8	1.4
Viscosity/ Alloys	A (Pa·s)	u (A)	E_a ($J \cdot mol^{-1}$)	u (E_a)	η (700°C) (Pa·s)	s (η)
Al [29]	0.191		14982.4		1.277	
Al5.0Mg0.2Sc3.0Li	0.168	0.006	16834.5	34.6	1.349	-0.001
Al5.0Mg0.2Sc6.0Li	0.181	0.010	16882.9	45.3	1.458	-0.010

[a] Estimated from linear regression error as implemented in the Grapher Software Package.
[b] Estimated from difference computed between experimental and calculated from linear density fit, $s(m)=\frac{1}{N}\sum_{i=1}^{N}\left|m^{exp}-m^{fit}\right|$, where N is the number of experimental points and standard deviation of density s(ρ), surface tension s(σ) and viscosity s(η).
[c] Standard uncertainties u are u(T) = 1 K, u(p) = 0.1 kPa at atmospheric pressure p = 0.1 MPa, w(X) = 0.0001 for Al, Mg and w(X) = 0.001 for Sc, Li.

The calculated density for Al4.6Mg0.66Sc0.42Zr0.49Mn [37] using linear thermal expansion show similar value as obtained for Al5.0Mg0.2Sc3.0Li alloy. The calculated value from model for surface tension of Al4.6Mg0.66Sc0.42Zr0.49Mn alloy [37] has much higher value 977 ($mN \cdot m^{-1}$) compare to this study 723.1 ($mN \cdot m^{-1}$) for Al5.0Mg0.2Sc3.0Li and 632.6 ($mN \cdot m^{-1}$) for Al5.0Mg0.2Sc6.0Li, at temperature 1173 K. The higher value it could be caused the taken of higher value of pure Al from [38]. The alloying elements and increasing Li in alloys caused increasing the viscosity compare to pure Al, the different character obtained in [37] for Al4.6Mg0.66Sc0.42Zr0.49Mn alloy, where calculate viscosity data, are lower. The obtained such low value of viscosity it could be caused by using a lower value of viscosity for

pure elements. However, similar to this study (Fig. 1c) the increase of viscosity for Al-Li [30], was observed. The higher value of viscosity is caused by the formation of IMCs from Al-Li system, correlate with short-range ordering in the liquid what was confirm by measurements and modelling [30].

3.2 Calorimetry study

The result from calorimetry study in the Fig. 2 as heating (a) and cooling (b) curves are presented. The addition 5 (wt%) of Mg to Al caused to the presented characteristic reaction from the Al-Li-Mg system. The obtained results have very good agreement with literature data for Al-Li-Mg system [39-43]. The phase diagram Al-Li [41, 42] and Al-Li-Mg [43], are presented in the Fig. 3, with the corresponding chemical composition of investigate alloys, respectively. For both alloys in the calorimetry curve first reaction around 540 $^{\circ}$C is start of dissolving ternary phase Al_2LiMg, which correspond reaction L + AlLi <=> (Al) + Al_2LiMg at 536 $^{\circ}$C [40]. Next in the DSC signal observed different temperature of reactions caused by different Li additions, which is correlated with phase diagram (Fig. 3). For 3 (wt %) of Li content the next peaks are observed at ~620 and ~631 $^{\circ}$C, which are correspond (Fig. 3a) to move to (Al) + L semisolid phase and next to liquid L. For the AlMgSc alloys with 6 (wt%) of Li content the different reactions are observed compare to 3 (wt %) Li, the two peaks are shown but in the lower temperature, first peak ta ~580 $^{\circ}$C could be correspond eutectic reaction from Li-Mg system L <=> (Mg) + (Li) at 588 $^{\circ}$C [44-46]. The next one around 600 $^{\circ}$C is from the eutectic reaction in Al-Li system, L <=> (A1) + AILi, which is in the same temperature 600 $^{\circ}$C [41], 602 $^{\circ}$C [40] or 596 $^{\circ}$C [44]. During cooling Fig. 2b, for both alloys the peak from crystallization was obtained, close to melting Al, as shown in Fig. 3, the expanding of the peak for AlMgSc with 6 (wt%) Li is correlated with the higher concentration of Li in the alloy. There is no effect after crystallization which means that obtained effect during heating is correlated with rapidly solidified process during droplet production. In the ternary Al-Li-Mg alloys, according to phase diagram (Fig. 3b) the equilibrium structure consists of (Al) grains with secondary particles of Al and Al_2LiMg phases formed during cooling in the solid state. The magnesium at early stages of decomposition is the reduced solid solubility of Li, what increasing density of precipitation of AlLi. Also, the magnesium and lithium form the ternary compound Al_2LiMg which is incoherent and nucleation on grain boundaries or dislocation networks. However, taking into account the chemical composition of alloys which have 0.2 Sc (wt %) what caused occurring the Al_3Sc according to phase diagram (Fig. 3c). The chemical composition of study alloys is corresponds to

Al5.0Mg0.2Sc3.0Li alloy the area of (Al) + Al_3Sc + Al_2LiMg and for Al5.0Mg0.2Sc6.0Li alloy the (Al) + Al_3Sc + AlLi + Al_2LiMg. The Sc addition caused stabilization of structure, considerably slows down lithium diffusion and coarsening of Al_3Li or AlLi phases and also stabilized the Al_2LiMg which could create at high Li concentrations. Moreover, the presence in the structure of coherent or semicoherent Al_3Sc (cubic particles) provides places for preferential nucleation of the Al-Li phases. To analyze the results from the different heating rate for Al5.0Mg0.2Sc6.0Li alloy as shown in the Fig 2c, before the main peak of described reaction there are some characteristic reactions in much lower temperature are presented. First peak is correspond to eutectic reaction at 418 $^{\circ}$C which is L <=> (Mg) + $Mg_{17}Al_{12}$ + AlLi [40]. The second one start around 485 $^{\circ}$C which correspond invariant reactions U_2 [40] at 483 $^{\circ}$C, L + Al_2LiMg <=> (Al) + $Mg_{17}Al_{12}$. The higher heating rate from 5 to 40 $^{\circ}$C/min little shift the peak of characteristic reaction to a lower temperature (Fig. 2c) which are correspond the presented precipitates from Al-Sc-Li-Mg system in microstructure described in next section.

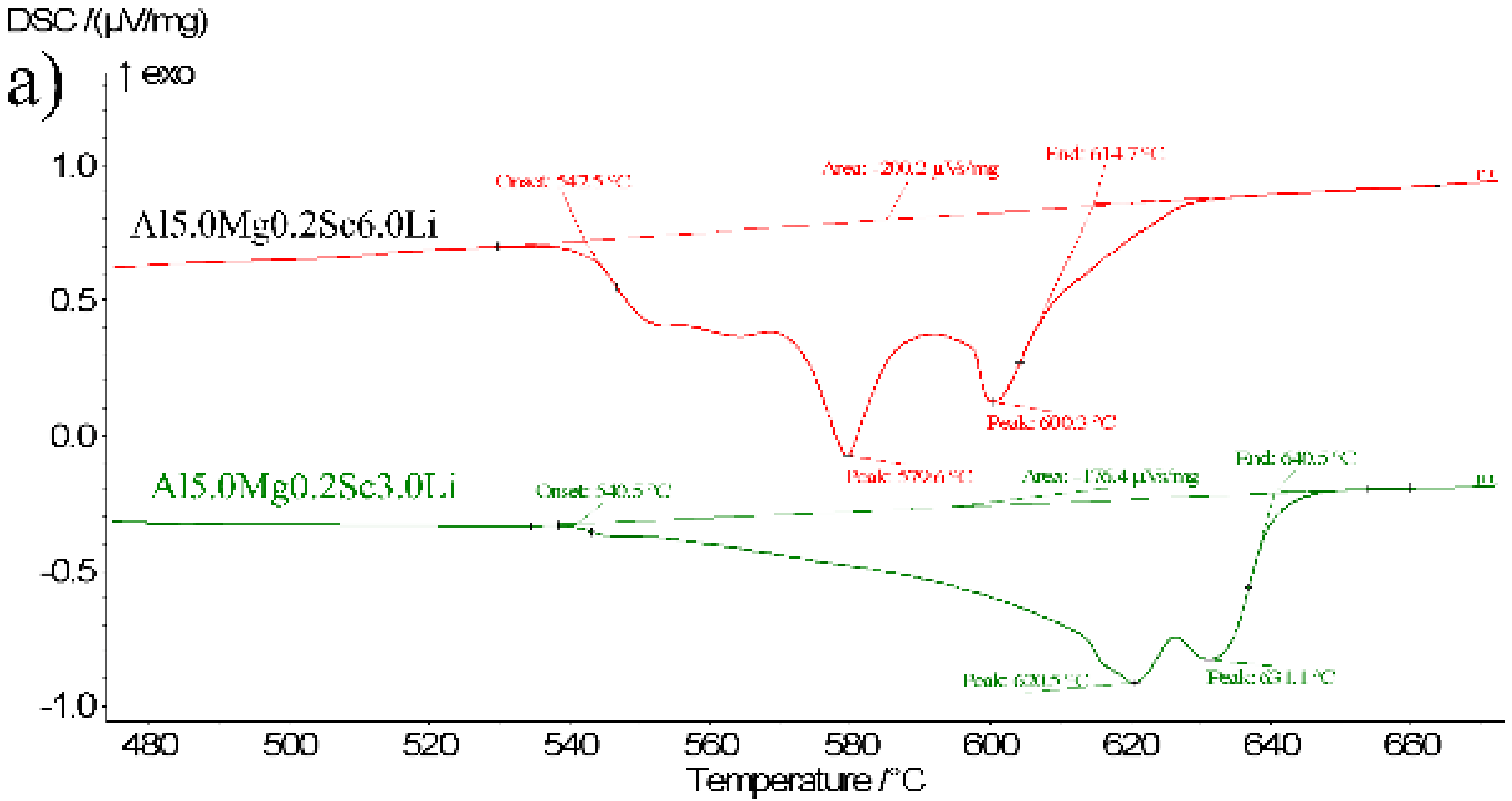
DSC /(μV/mg)
a)
↑ exo
1.0
0.5
0.0
-0.5
-1.0
Al5.0Mg0.2Sc6.0Li
Onset: 542.5 °C
Area: -200.2 μVs/mg
End: 614.7 °C
Peak: 600.2 °C
Peak: 579.6 °C
Al5.0Mg0.2Sc3.0Li
Onset: 540.5 °C
Area: -138.4 μVs/mg
End: 640.5 °C
Peak: 620.5 °C
Peak: 634.1 °C
480
500
520
540
560
580
600
620
640
660
Temperature /°C

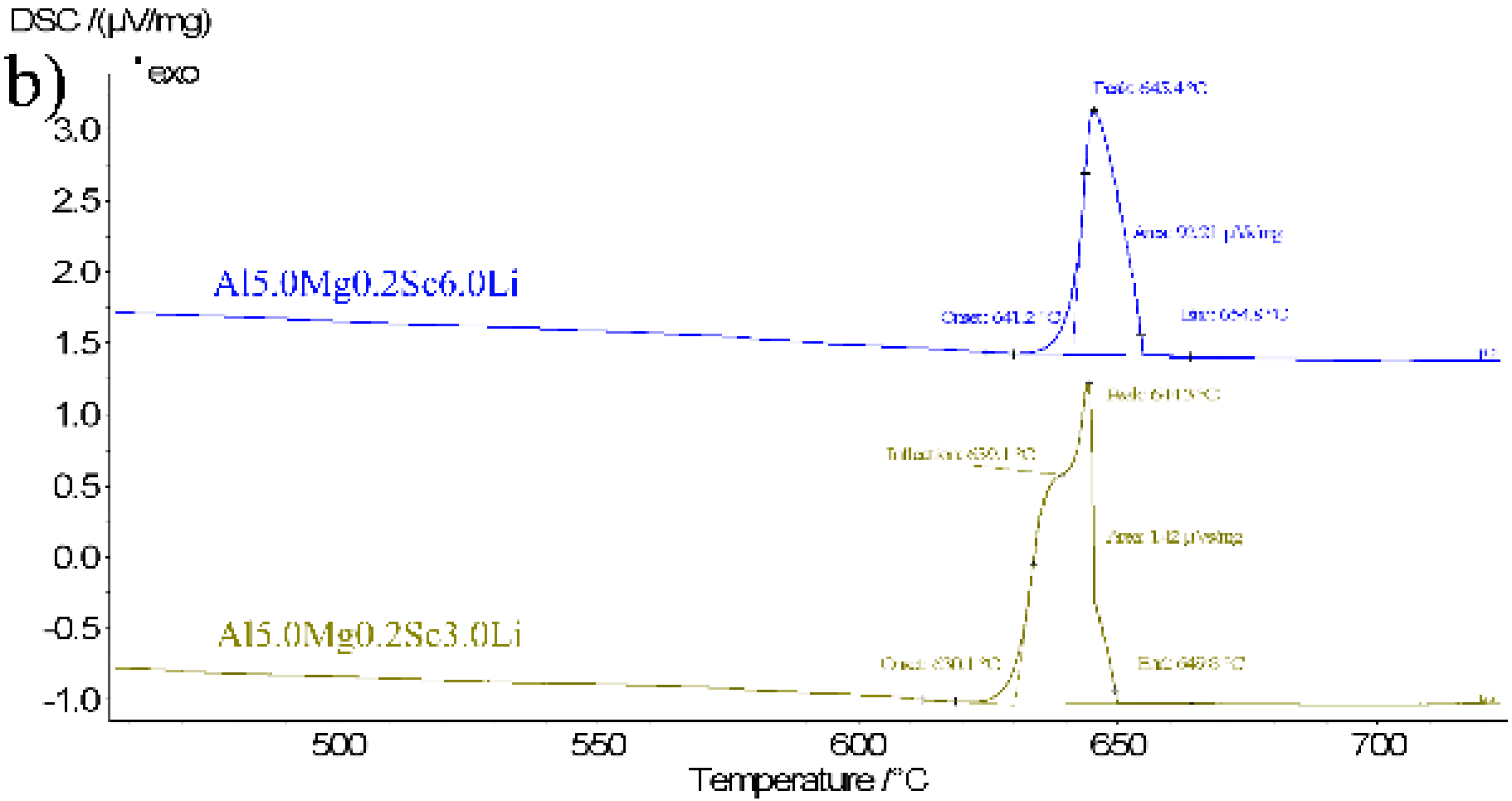
b)
DSC /(μV/mg)
exo
3.0
2.5
2.0
1.5
1.0
0.5
0.0
-0.5
-1.0
Al5.0Mg0.2Sc6.0Li
Al5.0Mg0.2Sc3.0Li
500
550
600
650
700
Temperature /°C

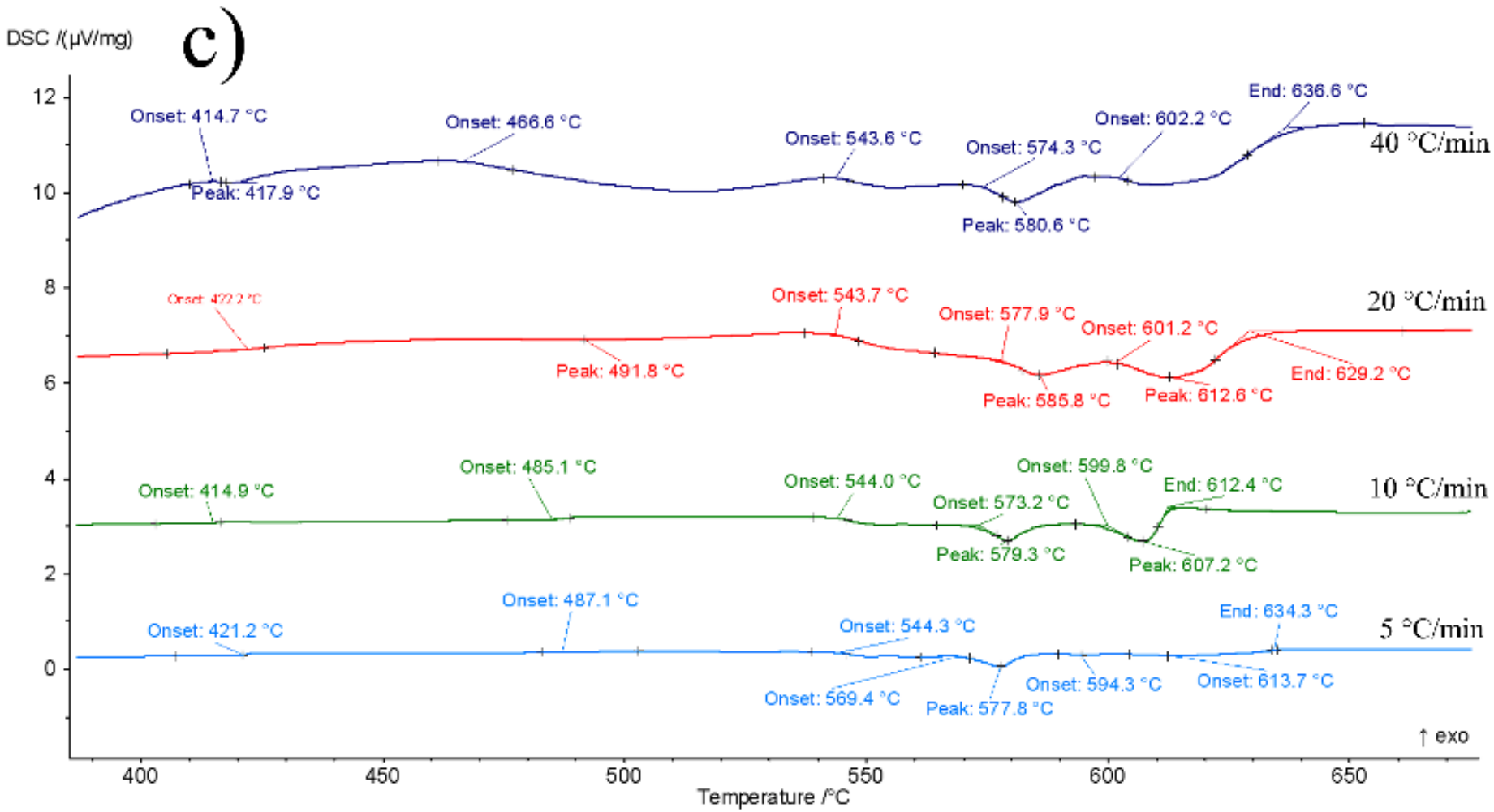
c)
DSC /(µV/mg)
12
10
8
6
4
2
0
Onset: 414.7 °C
Peak: 417.9 °C
Onset: 466.6 °C
Onset: 543.6 °C
Onset: 574.3 °C
Peak: 580.6 °C
Onset: 602.2 °C
End: 636.6 °C
40 °C/min
Onset: 422.2 °C
Peak: 491.8 °C
Onset: 543.7 °C
Onset: 577.9 °C
Peak: 585.8 °C
Onset: 601.2 °C
Peak: 612.6 °C
End: 629.2 °C
20 °C/min
Onset: 414.9 °C
Onset: 485.1 °C
Onset: 544.0 °C
Onset: 573.2 °C
Peak: 579.3 °C
Onset: 599.8 °C
Peak: 607.2 °C
End: 612.4 °C
10 °C/min
Onset: 421.2 °C
Onset: 487.1 °C
Onset: 544.3 °C
Onset: 569.4 °C
Peak: 577.8 °C
Onset: 594.3 °C
Onset: 613.7 °C
End: 634.3 °C
5 °C/min
↑ exo
400
450
500
550
600
650
Temperature /°C

Fig. 2. The DSC curve vs. temperature for AlMgSc with Li content alloys: a) during heating, b) cooling conditions, and for c) different heating rate from 5 to 40 ˚C/min of Al5.0Mg0.2Sc6.0Li alloy.

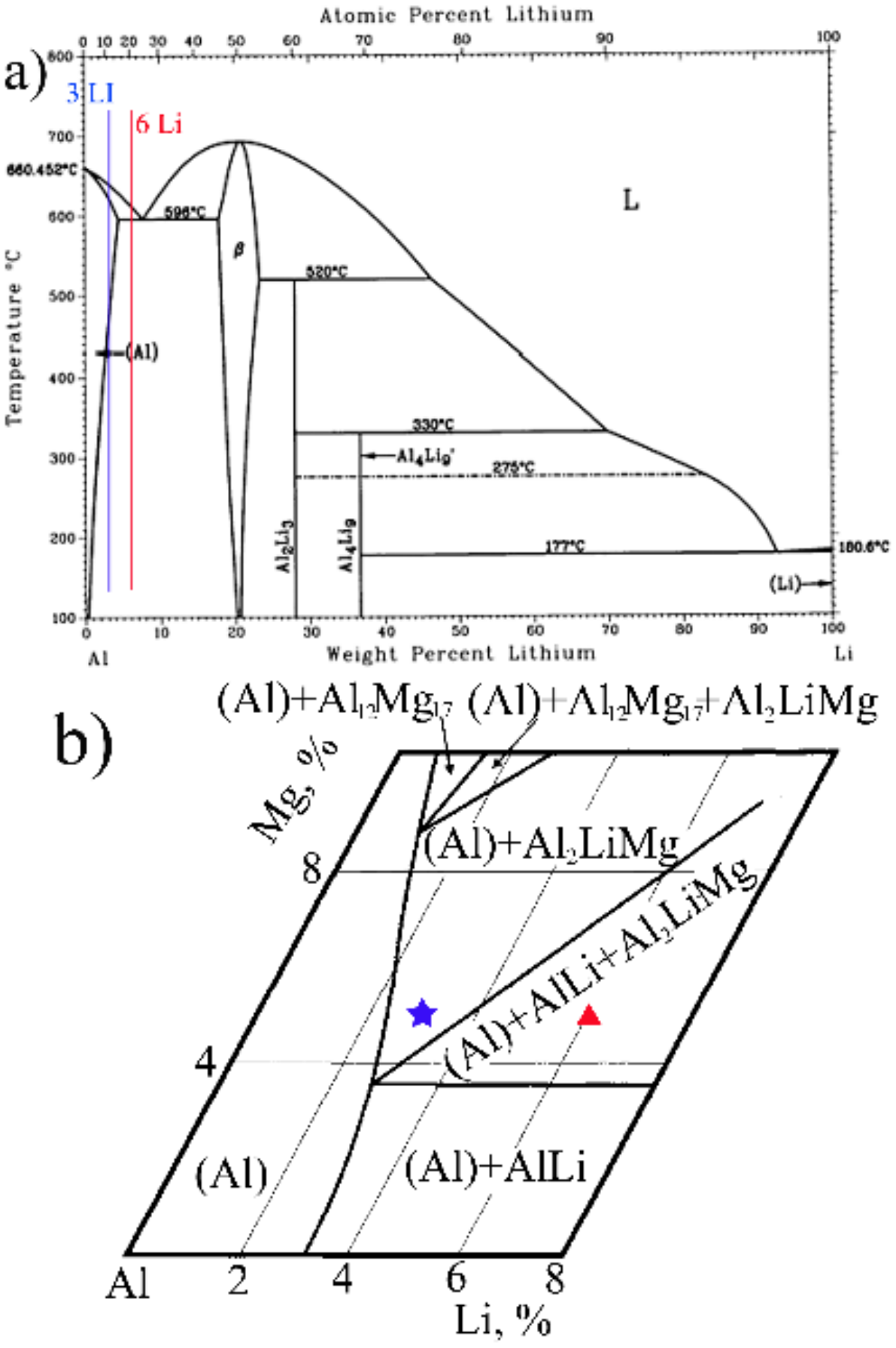
a)
Atomic Percent Lithium
Weight Percent Lithium
Temperature °C
Al
Li
3 Li
6 Li
660.452°C
596°C
β
L
520°C
(Al)
330°C
Al4Li9'
275°C
Al2Li3
Al4Li9
177°C
180.6°C
(Li)
b)
(Al)+Al12Mg17
(Al)+Al12Mg17+Al2LiMg
Mg, %
8
(Al)+Al2LiMg
(Al)+AlLi+Al2LiMg
4
(Al)
(Al)+AlLi
Al
2
4
6
8
Li, %

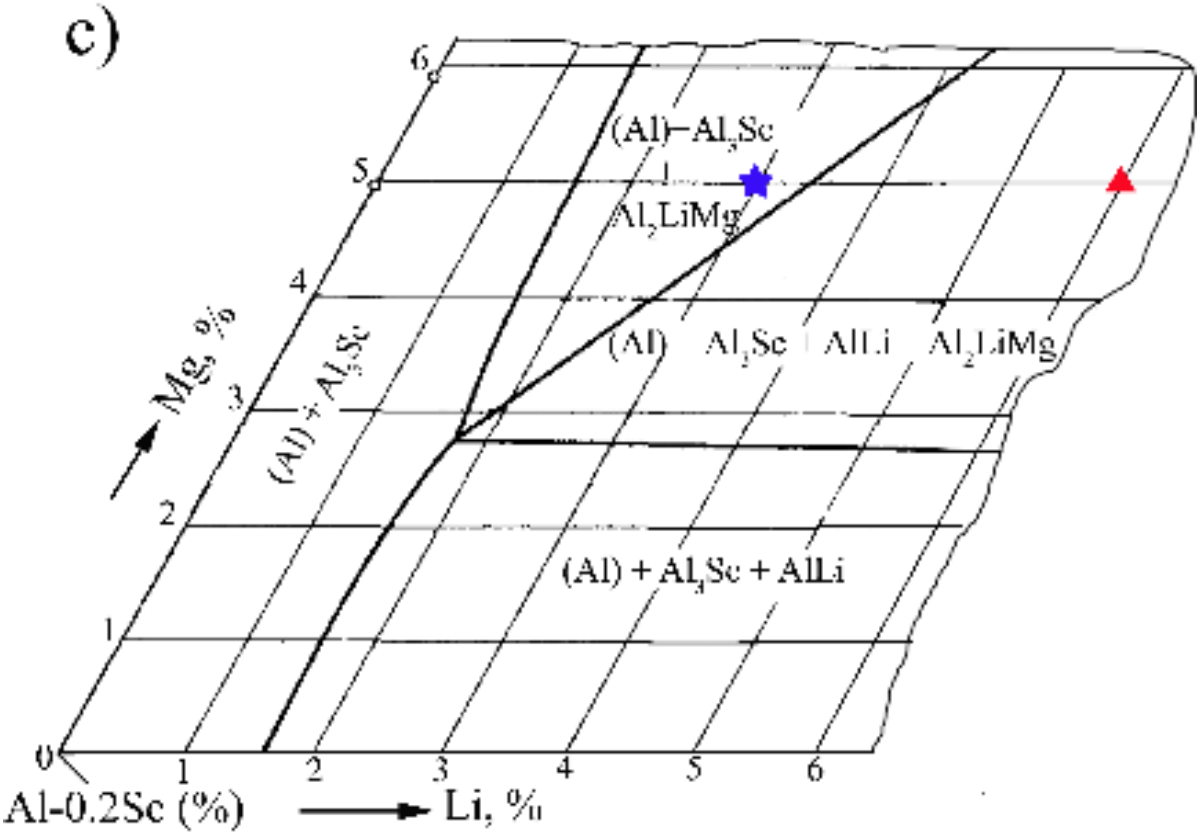

Fig. 3. The phase diagram of a) Al-Li [41, 42] and b) isothermal section of Al-Li-Mg at 500 ˚C [43] and c) isothermal section of Al0.2Sc-Li-Mg at 400 ˚C [47] with the signed chemical composition of investigated alloys.

3.3 Microstructure and XRDs

The microstructures of obtained droplets are present in Fig. 4 a, b) for Al5.0Mg0.2Sc3.0Li alloy and c, d) for Al5.0Mg0.2Sc6.0Li alloy, respectively. The microstructure is different for each alloys, in the case of 6 (wt %) Li the higher amount of precipitates are observed, compare to Al5.0Mg0.2Sc3.0Li alloy. The obtained microstructure for Al5.0Mg0.2Sc3.0Li alloy after rapid solidification looks very similar that the microstructure obtained after solution treated at 570 ˚C by 20h [48]. As shown in [49] the microstructures of cast ingots exhibiting ternary peritectic reactions are very often typical of non equilibrium type reactions what caused formed a border of the second phase forming around the primary phase as shown in (Fig. 2b). According to micro-segregation the Scheil-type the prediction of the final composition of the solidification is meaningful [50] which could along to monovariant lines as was analyzed in [51] for Al-Li-Cu system. In the microstructure of Al5.0Mg0.2Sc3.0Li is observed Al matrix with small precipitates Al_3Sc and Al_2LiMg and Mg on the grain boundary,

which is show in Fig. 5. The secondary electron micrographs and EDS elemental maps for Al, Mg, and Sc were done. On the EDS maps, the dispersion of Sc in the entire volume of the sample is shown, the Al formed grain and Mg occurred at the grain boundary, the same as observed in [37].

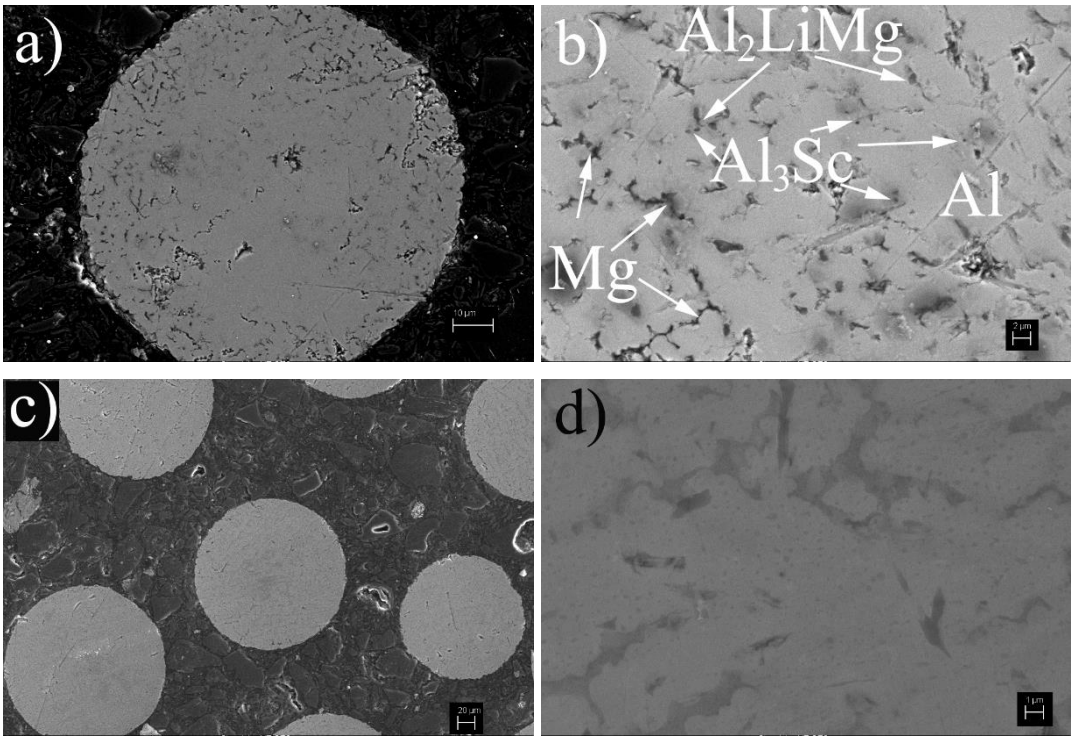

Fig. 4. The SEM microstructure of produced droplet a) and b) Al5.0Mg0.2Sc3.0Li with higher magnification, c) and d) Al5.0Mg0.2Sc6.0Li with higher magnification.

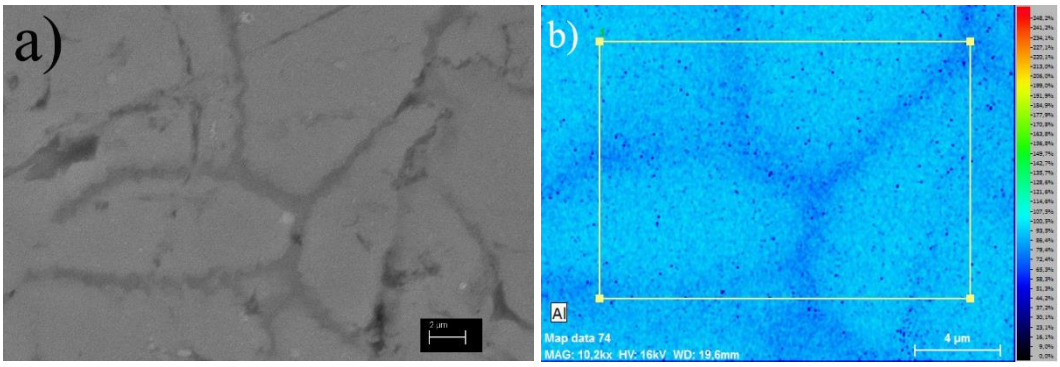

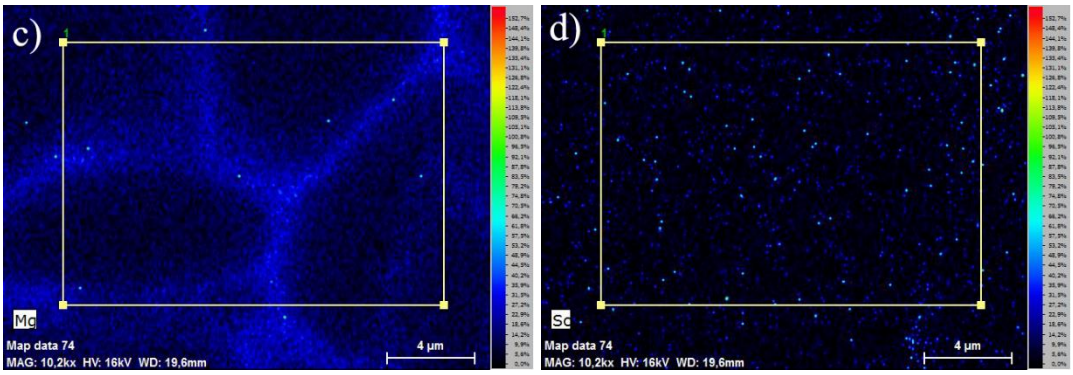

Fig. 5. The SEM microstructure and EDS maps of Al5.0Mg0.2Sc3.0Li alloy.

The conducted chemical analysis in SEM for Al5.0Mg0.2Sc3.0Li alloy, presented in Fig. 5, show that the Mg occurring at the grain boundary and Sc is distributed throughout the volume. The Sc is located both at grain boundaries and in the Al-grains. The higher concentration of Sc inside the Al grains is not observed. The same Sc distribution in [52] for Al5Mg0.2Sc cast alloy was observed, but with increasing Sc content to 0.4-0.6 caused formed square small precipitates Al_3Sc. However, the occurring the Al_3Sc precipitates should be more visible after the temperature treatment as show the literature data [37, 53]. Moreover, the addition of Mg and Sc at the level of 0.2 and 5.0 (wt %), respectively, caused occurring the Al_3Sc phase, which correspond to phase diagram Al-Mg-Sc [2], but the addition of Li introduces changes in the occurring phases (Fig. 3c) [47]. According to Al5.0Mg0.2Sc6.0Li alloy (Fig. 4d) in the microstructure much higher of small precipitates is observed, what with increasing Li content caused formed the precipitates of AlLi phase, according to phase diagram (Fig. 3c) [47].

The performed microstructure observation in TEM, presented in Fig. 6 showed the occurring small IMC precipitates at grain boundaries of Al grains and Mg regions. The microstructure observation similar as in [54] shows that the Mg addition causes substantial grain refinement of aluminum while Sc content in the form of a very fine dispersion of Al_3Sc precipitates is very efficient in restricting the grain growth. The presented in Fig. 8 microstructure in SEAD and after the electron diffraction patterns identify the occurring precipitates as Al_3Sc, AlLi and Al_2MgLi phases, which is in the line with the phase diagram presented in Fig. 3c. The selected precipitates in the Fig. 6, could be AlLi and Al_2MgLi phases as was identified in Fig. 8 and by SR-XRDs presented in Fig. 9. The microstructure of

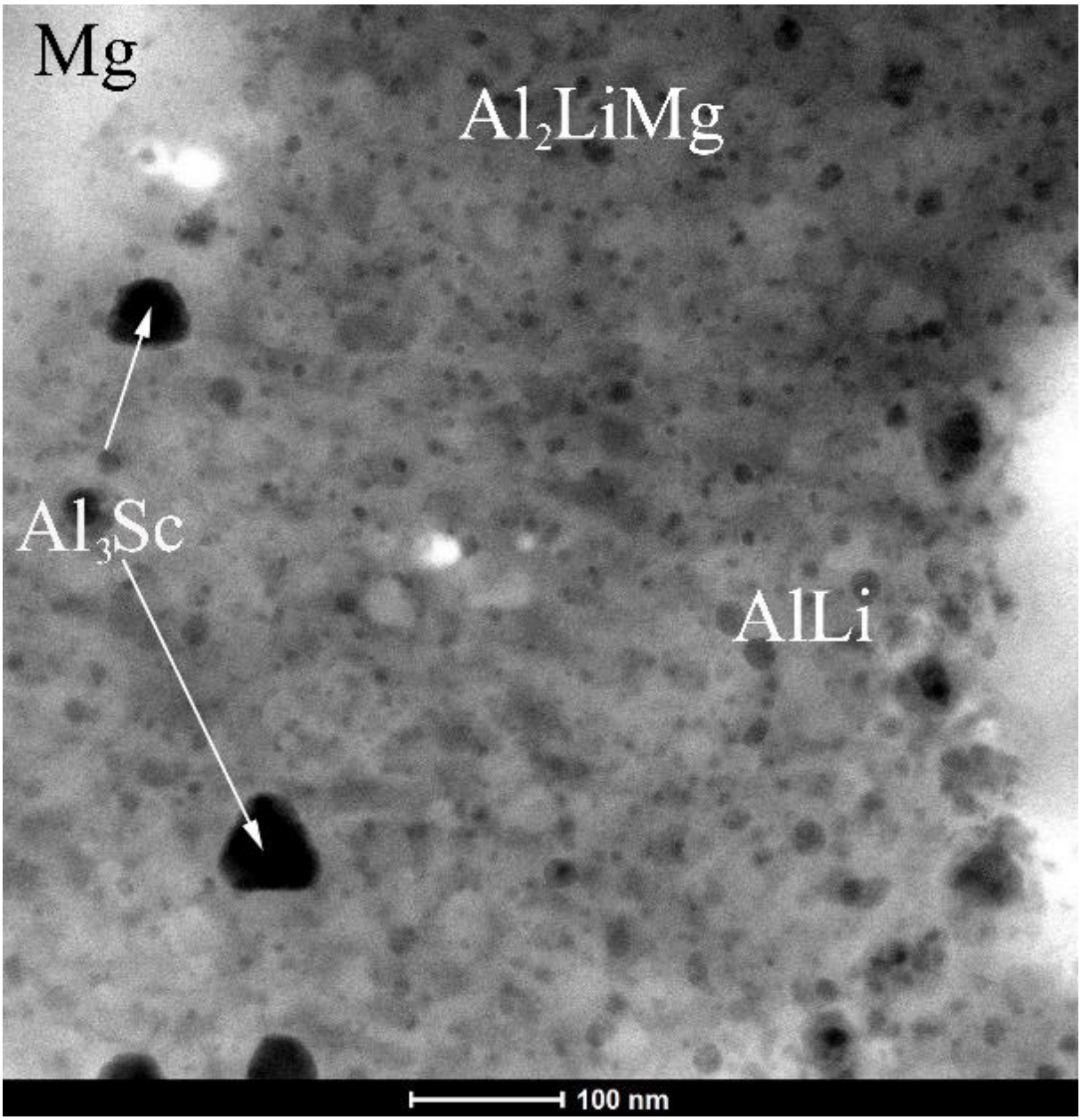

Fig. 6. The microstructure HAADF in TEM , of Al5.0Mg0.2Sc6.0Li alloy.

The conducted HAADF in TEM presented in Fig. 7 shows the maps of concentration occurring elements. The occurring Mg regions (Fig. 7c) are dendritic like/diffuse shaped of varying sizes doped by Al and Sc. Taking into account that the characterisation of Li is very difficult using HAADF-STEM, the occurring AlLi and Al_2MgLi phases was confirmed by electron diffraction patterns using TEM and SR-XRDs. The similar precipitate of AlLi phase as presented in Fig. 6, was observed by Noble and Thompson [55] and Prasad et al. [56]. According to Al_2MgLi phase, as reported in [56-58] the precipitates locating at the interdendrite spaces between the dendrite branches with a high enrichment of aluminum. The alloys with Li content shows two types of nucleation mechanisms [56]. First, the nucleation on the AlLi phase occurring at the matrix interface and with Mg concentrations occur at the

growth front. These excesses, combined with the excess vacancies released when Mg adds to the AlLi precipitate, result in a favorable condition for Al_2MgLi nucleation. The second nucleation on matrix dislocations and on subgrain boundary dislocations. In [56] was concluded that in Li-containing alloys, the dominant nucleation sites were grain boundary and dislocations. Therefore, as shown in phase diagram Fig. 3 and from Fridlyander et al. [59] study the addition of Li and Mg, the solubility of Sc in Al is decreased and this promotes the formation of Al_3Sc and the grain size and shape are also affected by the casting variables, such as cooling rate, superheat of the melt, stirring.

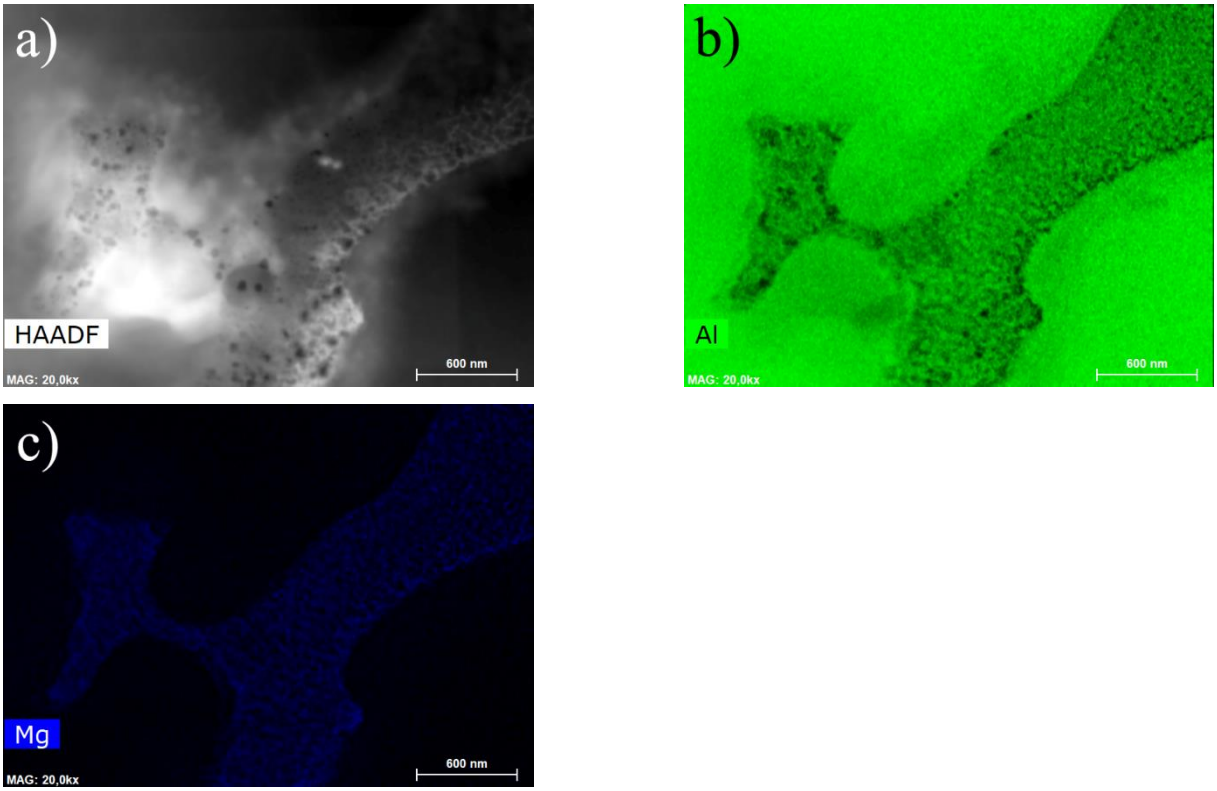

Fig. 7. A) HAADF-STEM image of Al5.0Mg0.2Sc6.0Li alloy and corresponding EDS maps for b) Al, c) Mg concentration.

According to phase diagram presented in Fig. 3, the identity of obtained phases existing after atomization process was using data presented in the literature [52, 56, 57, 60], the occurring phases presented in the Fig. 8. The crystallographic structure of the Al_3Sc phase was taken from [61], for AlLi from [62] and for Al_2MgLi from [57, 60, 63].

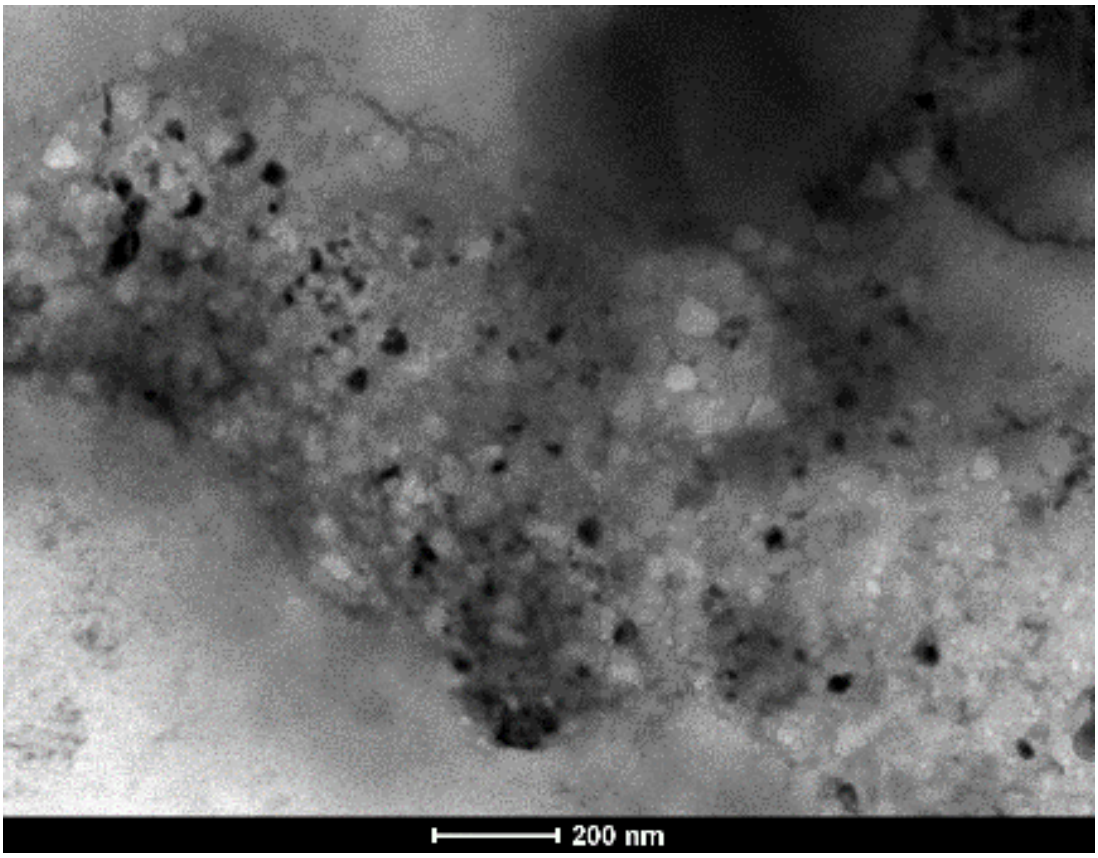
200 nm

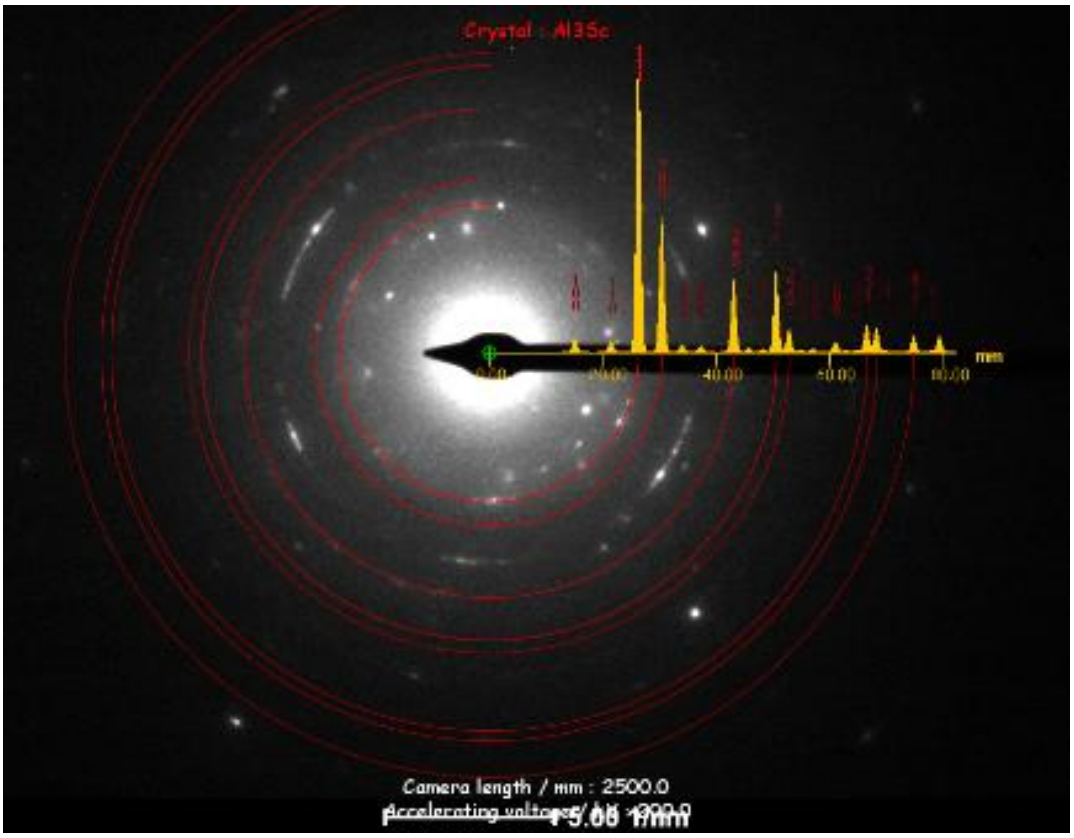
Crystal : Al3Sc
mm
Camera length / mm : 2500.0
Accelerating voltage / kV : 200.0
5.00 1/nm

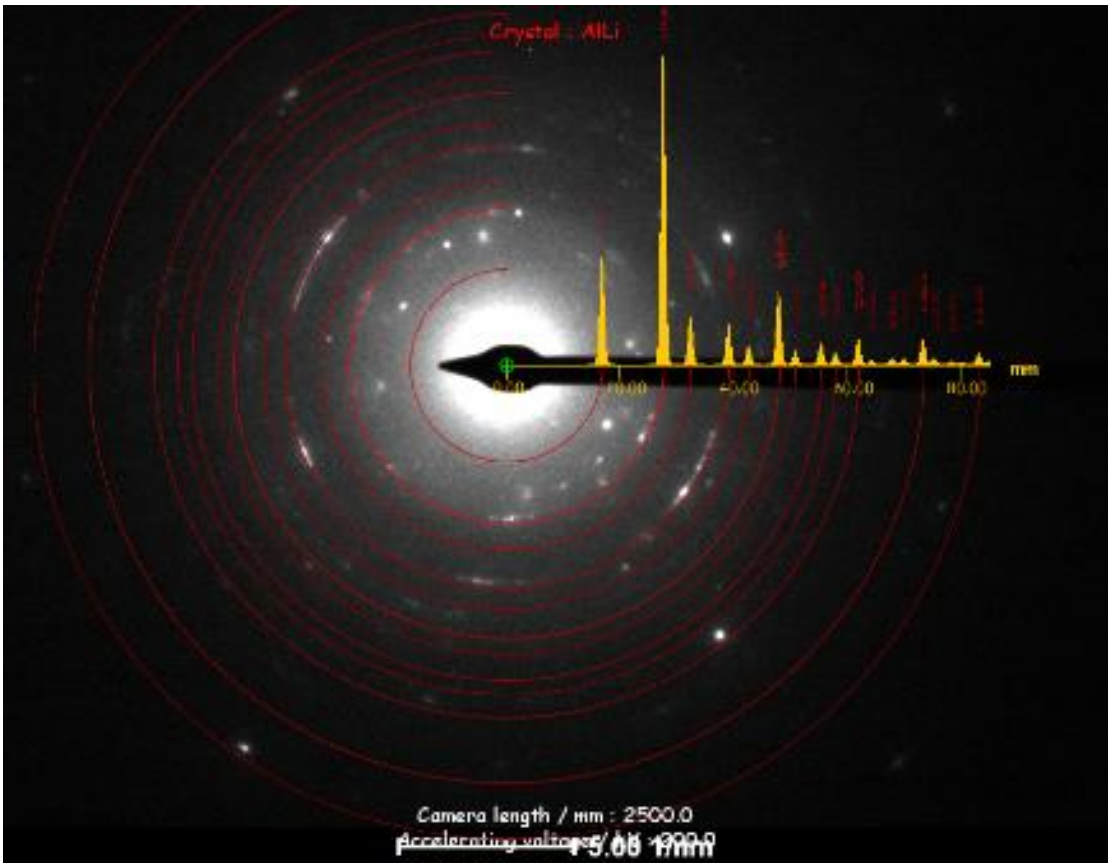
Crystal : AlLi
mm
Camera length / mm : 2500.0
Accelerating voltage / kV : 200.0
5.00 1/nm

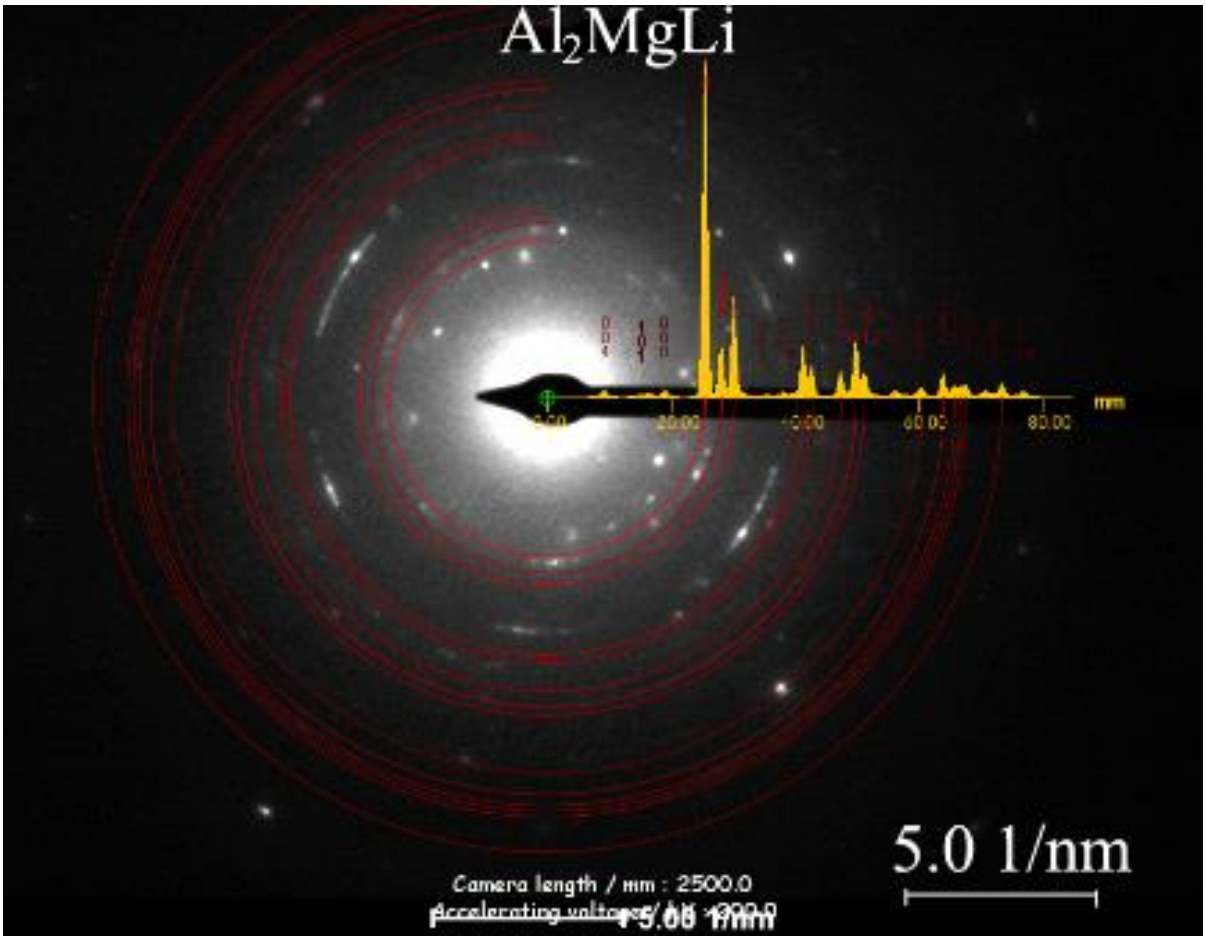

Fig. 8. The microstructure of Al5.0Mg0.2Sc6.0Li alloy was identified by SAED and electron diffraction patterns of the Al_3Sc, AlLi, and Al_2MgLi phases.

The conducted SR-XRD measurements for Al5.0Mg0.2Sc3.0Li and Al5.0Mg0.2Sc6.0Li alloys, for two sizes of droplets fine was 425-500 μm and coarse was 1.18-1.4 mm. The obtained SR-XRD results show that the size is the same for both droplets . Two curves are presented for Al5.0Mg0.2Sc6.0Li alloys (for two droplet size) and one for Al5.0Mg0.2Sc3.0Li alloy in Fig. 9. To characterize obtained SRXRD results, attribute the peak to phases, the higher magnification of SRXRD was needed without highest peak from Al, as shown in Fig. 9b. The SRXRD shows that for Al5.0Mg0.2Sc3.0Li alloy not occurring the AlLi phase and the characteristic peaks from Al_2MgLi phase are shifted and respond to Al_2Mg phase. The parameters for Al_2MgLi phase [60, 63] where a = 20.2 (Å) and for identifications has influence equilibrium with Al or with Mg and AlLi which could increase parameter up to 1.5 %.

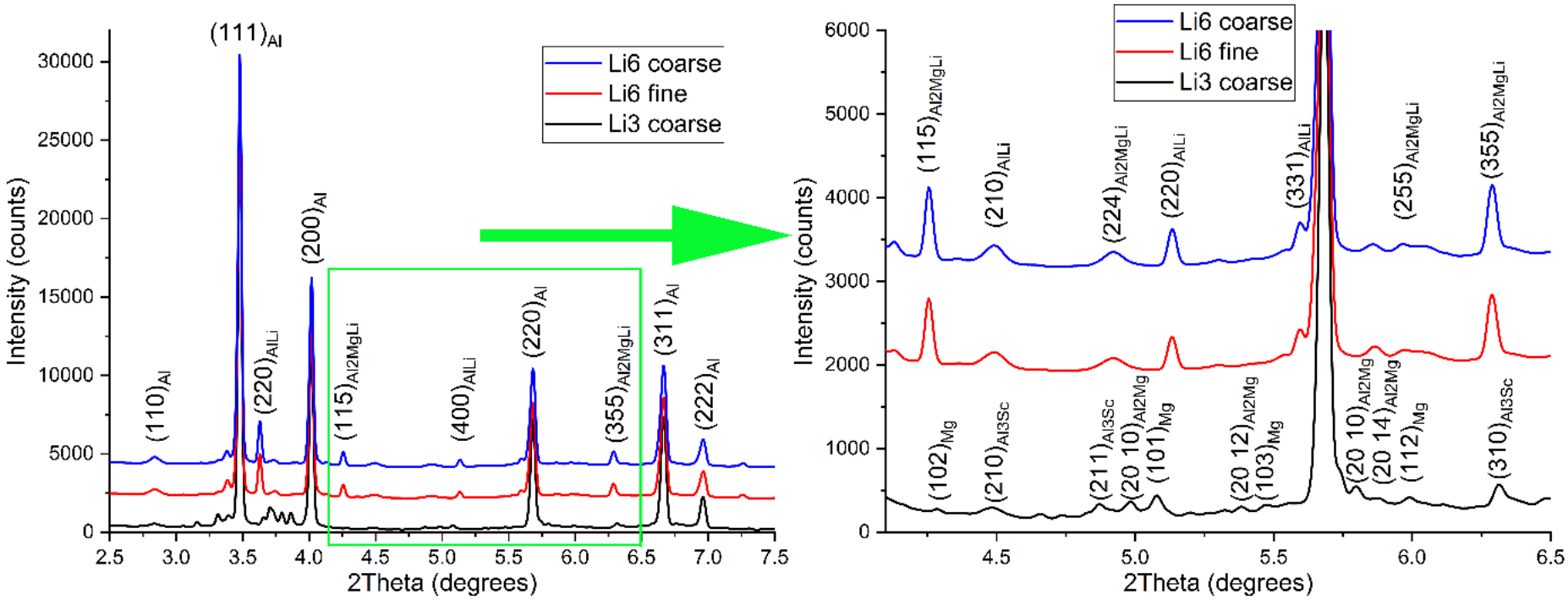

Fig. 9. The SR-XRD result for Al5.0Mg0.2Sc3.0Li and Al5.0Mg0.2Sc6.0Li alloys.

EBSD were carried out on the well-polished Al5.0Mg0.2Sc6.0Li droplets, due to the larger amount of precipitates. As an example, the EBSD phase distribution map is shown in Fig. 10. The complex phases has been identified by combining use of EBSD and EDS analysis. The Al and AlLi phases are very complicated due to similar crystal structure chemical composition. According to literature [60-63] in which is suggested that Al2MgLi and AlLi have a cubic structure with lattice parameters of 6.37 Å and 20.58 Å for a, respectively. Similarly, the Al phase also has a cubic crystal structure with lattice parameters of 4.04 Å for a. The slight difference between the lattice parameter make the phase identification more difficult. The Al_3Sc phase was not observed due to the small size of coherent particles appearing on the STEM-HAADF images. The legend next to the map shows that three phases were identified; aluminium, Al2MgLi and AlLi.

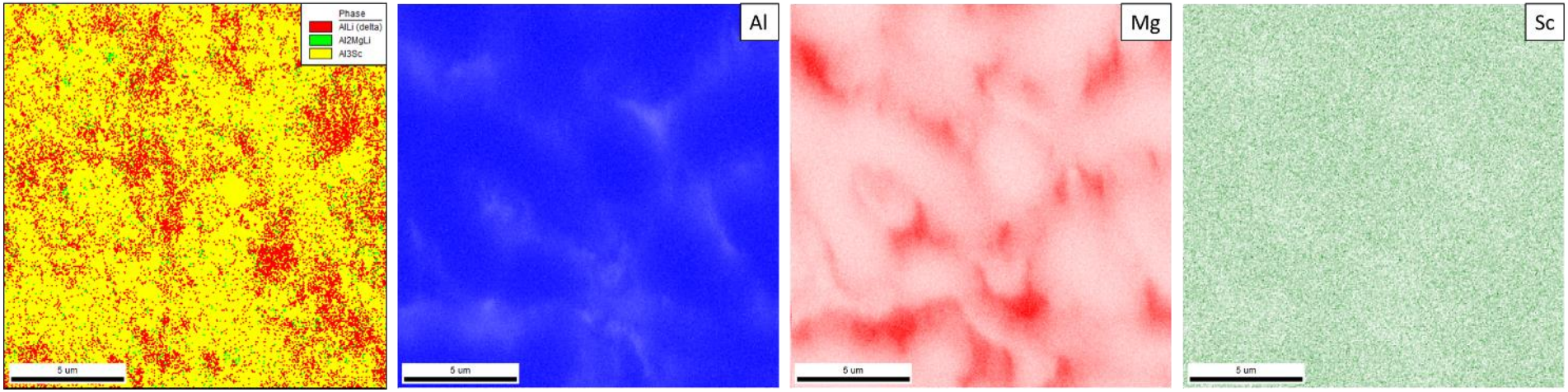

Fig. 10. EBSD results showing all selected phases.

4. Conclusions

In this study, the experiments were designed to shows the influence of Li addition to AlMgSc alloys on the thermophysical properties and microstructure observation after atomisation process. The fallowing conclusion can be drawn:

1. The density and surface tension decreases with increases Li content, opposite shows the viscosity which also increase. The higher value of viscosity compare to Al-Li alloys it could be caused by formed IMCs not only from Al-Li system, but also ternary phase as Al_2MgLi.
2. The occurring Al_2MgLi phase was confirmed by analysis using electron diffraction patterns in TEM and SR-XRDs. The obtained results are in the line with phase diagram of Al-Li-Mg system (Fig. 3) and with the literature [57, 60, 63].
3. The obtained droplets after atomization process for Al5.0Mg0.2Sc3.0Li alloy characterize occurring Al_3Sc and Al_2MgLi phases at grain boundaries of Al grains and at Mg regions. The microstructure observation for Al5.0Mg0.2Sc6.0Li alloy shows occurring another AlLi phase as small precipitates inside the Al grains.
4. The performed calorimetry study shows similar character obtained of temperature phase transformations, however, there are specific differences between obtained DSC curve for Al5.0Mg0.2Sc3.0Li and Al5.0Mg0.2Sc6.0Li alloys. The obtained results confirmed proposed of the phase diagram of Al-Li-Mg system, presented in Fig. 3.
5. The occurring IMCs Al_3Sc and Al_2MgLi phases for Al5.0Mg0.2Sc3.0Li alloy and Al_3Sc, AlLi and Al_2MgLi phases for Al5.0Mg0.2Sc6.0Li alloy were confirmed by electron diffraction patterns in TEM and SR-XRDs.

Acknowledgment

This work is the results of cooperation between Department of Chemical and Materials Engineering, University of Alberta and Institute of Metallurgy and Materials Science, Polish Academy of Sciences.

References

1. A. Deschamps, C. Sigli, T. Mourey, F. de Geuser, W. Lefebvre, B. Davo, Experimental and modelling assessment of precipitation kinetics in an Al–Li–Mg alloy, Acta Materialia 60 (2012) 1917–1928
2. J. Røyset, N. Ryum, Scandium in aluminium alloys, Int. Mater. Rev. 50 (2005) 19–44A
3. Deschamps, G. Fribourg, Y. Bréchet, J.L. Chemin, C.R. Hutchinson, In situ evaluation of dynamic precipitation during plastic straining of an Al–Zn–Mg–Cu alloy, Acta Materialia 60 (2012) 1905–1916
4. Yu. Buranova, V. Kulitskiy, M. Peterlechner, A. Mogucheva, R. Kaibyshev, S.V. Divinski, G. Wilde, Al3(Sc,Zr)-based precipitates in Al–Mg alloy: Effect of severe deformation, Acta Materialia 124 (2017) 210–224
5. G. Guillemot, C-A. Gandin, Analytical model for equiaxed globular solidification in multicomponent alloys, Acta Materialia 97 (2015) 419–434
6. J.E. Hatch, Aluminum: Properties and Physical Metallurgy, ASM International, 1984.
7. M. Bedel, G. Reinhart, A.-A. Bogno, Ch.-A. Gandin, S. Jacomet, E. Boller, H. Nguyen-Thi, H. Henein, Characterization of dendrite morphologies in rapidly solidified Al–4.5 wt.%Cu droplets, Acta Materialia 89 (2015) 234–246
8. S.J. Savage, F.H. Froes, Production of rapidly solidified metals and alloys, J. Metals (1984) 20–33
9. A. Lawley, An overview of powder atomization processes and fundamentals, Int. J. Powder Metall. Powder Technol. 2 (1977) 169–188
10. A. Prasad, H. Henein, E. Maire, C.-A. Gandin, Understanding the rapid solidification of Al–4.3Cu and Al–17Cu using Xray tomography, Metall. Mater. Trans. A 37 (2006) 249–257
11. H. Henein, V. Buchoud, R.-R. Schmidt, C. Watt, D. Malakov, C.-A. Gandin, G. Lesoult, V. Uhlenwinkel, Droplet solidification of impulse atomized Al–0.61Fe and Al–1.9Fe, Can. Metall. Q 49 (2010) 275–292
12. A. Ilbagi, H. Henein, A.B. Phillion, Phase quantification of impulse atomized Al68.5Ni31.5 alloy, J. Mater. Sci. 46 (2011) 6235–6242
13. A. Ilbagi, P. D. Khatibi, I.P. Swainson, G. Reinhart, H. Henein, Microstructural analysis of rapidly solidified aluminium–nickel alloys, Can. Metall. Q. 50 (2011) 295–302

14. E. A. Marquis, D. N. Seidman, M. Asta, C. Woodward, Composition evolution of nanoscale Al3Sc precipitates in an Al–Mg–Sc alloy: Experiments and computations, Acta Materialia 54 (2006) 119–130
15. L.S. Toporova, D.G. Eskin, M.L. Kharakterova, T.B. Dobatkina, Advanced aluminum alloys containing scandium, Gordon & Breach, Amsterdam (1998)
16. H.W. King, Quantitative size-factors for metallic solid solutions, J. Mater. Sci. 1 (1966) 79-90
17. G. L. Shneider, A. M. Drits, Hardenability of aluminum-lithium alloys, Met. Sci. Heat. Treat. 37 (1995) 373-377
18. R. R. Sawtell, C. L. Jensen, Mechanical Properties and Microstructures of AI-Mg-Sc Alloys, Metal. Trans. A 21 (1990) 421-430
19. D.H. Xiao, M. Song, F.Q. Zhang, Y.H. He, Characterization and preparation of Mg–Al–Zn alloys with minor Sc, J. Alloy Compd. 484 (2009) 416–421
20. J. Røyset, Scandium in Aluminium alloys overview: physical metallurgy, properties and applications, Metall. Sci. Tech. 25 (2007) 11-21
21. Y. Miura, K. Horikawa, K. Yamada and M. Nakayama, Proc. 4th Int. Conf. on Aluminum Alloys, Their Physical and Mechanical Properties, Vol. II, Atlanta, GIT, USA, September 1994, 161–168.
22. C.-H. Joh, K. Yamada, Y. Miura, Effect of Sc-Addition on the Coarsening Behavior of Al3Li Precipitates in Al-Li Alloys, Mater. Trans. JIM 40 (1999) 439–442.
23. Z. Ahmad, The properties and application of scandium-reinforced aluminium, JOM 55 (2003) 35-39.
24. M. Trybula, T. Gancarz, W. Gasior, A. Pasturel, Bulk and Surface Properties of Liquid Al-Li and Li-Zn Alloys, Metall. Mater. Trans. A 45 (2014) 5517-5530
25. T. Gancarz, W. Gasior, H. Henein, The Discharge Crucible Method for Making Measurements of the Physical Properties of Melts: An Overview, Int. J. Thermophys. 35 (2014) 1725–1748
26. T. Gancarz, Density, surface tension and viscosity of liquid ZnAl + X (X = Li, Na, Si) alloys, Fluid Phase Equilibr. 427 (2016) 97-103
27. T. Gancarz, Z. Moser, W. Gąsior, J. Pstruś and H. Henein, A comparison of surface tension, viscosity and density of Sn and Sn-Ag alloys using different measurement techniques, Int. J. Thermophys. 32 (2011) 1210-1233
28. T. Gancarz, W. Gasior, The effects of Na addition on the density, surface tension and viscosity of liquid Sn-Zn alloys, Fluid Phase Equilibr. 418 (2016) 57-61

29. T. Gancarz, J. Jourdan, W. Gasior, H. Henein, Physicochemical properties of Al, Al-Mg and Al-Mg-Zn alloys, Mol. Liq. 249 (2018) 470-476
30. M. Trybula, T. Gancarz, W. Gasior, Density, surface tension and viscosity of liquid binary Al-Zn and ternary Al-Li-Zn alloys, Fluid Phase Equilibr. 421 (2016) 39-48
31. M. Bedel, G. Reinhart, A.-A. Bogno, Ch.-A. Gandin, S. Jacomet, E. Boller, H. Nguyen-Thia, H. Henein, Characterization of dendrite morphologies in rapidly solidified Al–4.5 wt.%Cu droplets, Acta Materialia 89 (2015) 234–246
32. J.B. Wiskel, H. Henein, E. Maire, Solidification study of aluminum alloys using impulse atomization: Part I: heat transfer analysis of an atomized droplet, Can. Metall. Q. 41 (2002) 97–110.
33. H. Henein, Single fluid atomization through the application of impulses to a melt, Mater. Sci. Eng. A 326 (2002) 92–100
34. M.P.I. Federation, Standard Test Methods for Metal Powders and Powder Metallurgy Products 2012, Metal Powder Industry, S.l., 2012
35. B. Klöden, PhD-Thesis Institut für Strukturphysik, TU Dresden, 2006
36. M. J. Assael, K. Kakosimos, R. M. Banish, J. Brillo, I. Egry, A. Nagashima, Y. Sato, W. A. Wakeham, Reference Data for the Density and Viscosity of Liquid Aluminum and Liquid Iron, J. Phys. Chem. Ref. Data 35 (2006) 285-300
37. A.B. Spierings, K. Dawson, T. Heeling, P.J. Uggowitzer, R. Schäublin, F. Palm, K.Wegener, Microstructural features of Sc- and Zr-modified Al-Mg alloys processed by selective laser melting, Mat. Des. 115 (2017) 52–63
38. W. F. Galo, T. C. Totemeier, Smithells Metals Reference Book, Eight Edition, Elsevier and ASM International, (2004)
39. Nikolay A. Belov, Dmitry G. Eskin, Andrey A. Aksenov, Multicomponent Phase Diagrams: Applications for Commercial Aluminum Alloy, Chapter 8 Alloys with Lithium, ELSELVIER, (2005) ISBN: 0-080-44537-3
40. G. Ghosh, Al-Li-Mg (Aluminium - Lithium - Magnesium), Light Metal Systems. Part 3, Springer 2005, DOI: 10.1007/10915998_11
41. E. Schiirmann, I.K. Geissler, "Solid Phase Equilibrium in Mg-Rich Alloys of the Al-Li-Mg System," Giessereiforschung, 32(4)/163-174 (1980); also I.K Geissler's Ph.D. thesis, Tech. Univ. Clausthal (1979)

42. E. Schiirmann, HJ. Voss, "Investigation of the Melting Equilibria of Mg-Li-A1 Alloys," Giessereiforschung, 33(2), 33-53 (1981); also H.J. Voss' Ph.D. thesis, Tech. Univ. Clausthal (1979)
43. M.E. Drits, E.M. Padeznova, L.S. Guzei, "The Mg-Li-A1 Phase Diagram," Russ. Metall. 2 (1977) 167-170
44. N.C. Goel, J.R. Cahoon, The AI-Li-Mg System (Aluminum-Lithium-Magnesium), Bull. Alloy Phase Diagr. Vol. II No. 6 (1990) 528-546
45. A.A. Nayeb-Hashemi, J.B. Clark, A.D. Pelton, "The Li-Mg (Lithium-Magnesium) System" Bull. Alloy Phase Diagr. 5(4) (1984) 365-374
46. R. H. Taylor, S. Curtarolo, G. L. W. Hart, "Ordered Magnesium-Lithium Alloys: First-Principles Predictions, Phys. Rev. B 81 (2010) 24112-8
47. L.N. Fridlyander, L.L. Rokhlin, T.V. Dobatkina, N.L. Nikitina, Investigation of the phase equilibria in aluminum alloys containing lithium, Metalloved. Term. Obrab. Met. 10 (1993) 16-19.
48. Y. Peng, A. Chen, L. Zhang, W. Liu, and G. Wu, “Effect of solution treatment on microstructure and mechanical properties of cast Al–3Li–1.5Cu–0.2Zr alloy,” J. Mater. Res., vol. 31, no. 8, pp. 1124–1132, Apr. 2016.
49. B. Dubost, P. Bompard, I. Ansara. Experimental study and thermodynamic calculation of the al-li-mg equilibrium phase diagram, J. Phys-Parise. 48 (C3) (1987) C3-473-479.
50. T. Himemiya, “Micro-Segregation along the Monovariant Line in a Ternary Eutectic Alloy System, Metall. Trans. 44 (2003) 811-818.
51. S.-W. Chen, Y.-Y. Chuang, Y. A. Chang and M. G. Chu, Calculation of phase diagrams and solidification paths of Al-rich Al−Li−Cu alloys, Metall. Trans. 22A (1991) 2837–2848.
52. S. Zhou, Z. Zhang. M. Li, D. Pan, H. Su, X. Du, P. Li, Y. Wua, Effect of Sc on microstructure and mechanical properties of as-cast Al–Mg alloys, Mater. Des. 90 (2016) 1077-1084
53. S. Lee, A. Utsunomiya, H. Akamatsu, K. Neishi, M. Furukawa, Z. Horita, T.G. Langdon, Influence of scandium and zirconium on grain stability and superplastic ductilities in ultrafine-grained Al–Mg alloys, Acta Mater. 50 (2002) 553–564
54. K. Dam, P. Lejcek, A. Michalcova, In situ TEM investigation of microstructural behavior of superplastic Al–Mg–Sc alloy, Mater. Character. 76 (2013) 69-75
55. B. Noble, G.E. Thompson, Precipitation Characteristics of Aluminium-Lithium Alloys, Met. Sci. J. 5 (1971) 114-120

56. K. S. Prasad, N. E. Prasad, A. A. Gokhale, Chapter 4 – Microstructure and Precipitate Characteristics of Aluminum–Lithium Alloys, Aluminum-lithium Alloys, Processing, Properties, and Applications, 2014, 99–137
57. G.E. Thompson, B. Noble, Precipitation characteristics of aluminum–lithium alloys containing magnesium, J. Inst. Metals 101 (1973) 111-115
58. L. S. Kramer, T. J. Langan, J. R. Pickens, H. Last, Development of AI-Mg-Li alloys for marine applications, J. Mater. Sci. 29 (1994) 5826-5832
59. S. Kumar, H. B. McShane, T. Sheppard, Effect of zirconium and magnesium additions on properties of Al–Li based alloy, Mater. Sci. Tech. 10 (1994) 162-172
60. D.W. Levinson, D.J. McPherson, Phase Relations in Magnesium-Lithium-Aluminium Alloys, Trans. Amer. Soc. Met. 48 (1956) 689-705
61. J.C. Schuster, J. Bauer, The Ternary Systems Sc-Al-N and Y-Al-N, J. Less-Common Met., 109 (1985) 345-350
62. K. Kishio, J.O. Brittain, Phase Stability of Doped b-LiAl, Mater. Sci. Eng. 49 (1981) 1-6
63. T.V. Schegoleva, O. F. Rybalko, Структура метастабильной S'-фасе в сплаве Al-Mg-Li, Fiz. Met. Metalloved+. 50 (1980) 86-90 (in Russian)